ACS APPLIED MATERIALS & INTERFACES

Research Article

www.acsami.org

Poly(acrylic acid) Bridged Gadolinium Metal–Organic Framework–Gold Nanoparticle Composites as Contrast Agents for Computed Tomography and Magnetic Resonance Bimodal Imaging

Chixia Tian,[†] Liping Zhu,[†] Feng Lin,[‡] and Stephen G. Boyes*[,†]

[†]Department of Chemistry and Geochemistry, Colorado School of Mines, Golden, Colorado 80401, United States

[‡]Environmental Energy Technologies Division, Lawrence Berkeley National Laboratory, Berkeley, California 94720, United States

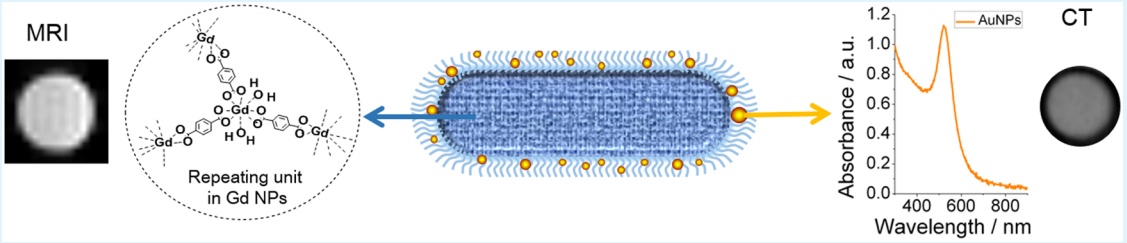

ABSTRACT: Imaging contrast agents for magnetic resonance imaging (MRI) and computed tomography (CT) have received significant attention in the development of techniques for early stage cancer diagnosis. Gadolinium (Gd)(III), which has seven unpaired electrons and a large magnetic moment, can dramatically influence the water proton relaxation and hence exhibits excellent MRI contrast. On the other hand, gold (Au), which has a high atomic number and high X-ray attenuation coefficient, is an ideal contrast agent candidate for X-ray-based CT imaging. Gd metal–organic framework (MOF) nanoparticles with tunable size, high Gd(III) loading and multivalency can potentially overcome the limitations of clinically utilized Gd chelate contrast agents. In this work, we report for the first time the integration of GdMOF nanoparticles with gold nanoparticles (AuNPs) for the preparation of a MRI/CT bimodal imaging agent. Highly stable hybrid GdMOF/AuNPs composites have been prepared by using poly(acrylic acid) as a bridge between the GdMOF nanoparticles and AuNPs. The hybrid nanocomposites were then evaluated in MRI and CT imaging. The results revealed high longitudinal relaxivity in MRI and excellent CT imaging performance. Therefore, these GdMOF/AuNPs hybrid nanocomposites potentially provide a new platform for the development of multimodal imaging probes.

KEYWORDS: *multimodal imaging contrast agent, MRI/CT, gold nanoparticles, gadolinium metal–organic framework nanoparticles*

INTRODUCTION

The integration of different functional materials into a single nanocomposite generates new opportunities to simultaneously achieve the collective functions of both materials and enable enhanced performance for a variety of emerging applications, including but not limited to catalysis,[1−4] renewable energy,[5,6] and biomedicine.[7−9] Specifically, multifunctional nanomaterials have been intensively studied in the area of biomedicine for drug/gene delivery,[10,11] diagnosis,[12,13] and monitoring of treatment.[14−16] The unique features of nanoparticles distinguish them from conventional small-molecule-based biomedicine. First of all, nanoparticles possess characteristic physicochemical properties, where multiple applications can be achieved in one single particle. For example, gold nanoparticles (AuNPs) with certain shape and size can be utilized in imaging as well as photothermal therapy.[16,17] Second, nanoparticles can be easily modified with other functionalities (e.g., polymer or targeting ligand) to realize multimodal properties.[16] One area in the biomedical field where nanoparticles have received considerable interest is in diagnostic imaging. Different types of nanoparticles have been investigated for various bioimaging applications, including natural structures (lipoproteins, viruses, and ferritin),[18] metals (Au, Ag, Pt),[19] metal oxides (Fe_3O_4, lanthanide oxide),[20,21] and semiconducting nanostructures (quantum dots),[22] where the specific nanoparticle chosen is dependent upon the desired imaging modality.

Widely used diagnostic imaging techniques include magnetic resonance imaging (MRI), X-ray-based computed tomography (CT), ultrasound, optical coherence tomography, single photon emission computed tomography (SPECT), and positron emission tomography (PET). Comprehensive diagnostic information is unlikely to be captured using a single technique due to the intrinsic limitations in each individual imaging technique.[23] Therefore, multimodal imaging techniques are being developed to integrate the advantages of various imaging techniques into one system. Common combinations include PET/CT,[24] MRI/PET,[25] CT/SPECT,[26] or MRI/optical imaging.[27] CT, one of the most common and cost-effective imaging techniques available clinically, gives high-resolution 3D tomography information anatomically but has limited soft

Received: May 8, 2015
Accepted: July 6, 2015
Published: July 6, 2015

DOI: 10.1021/acsami.5b03998
ACS Appl. Mater. Interfaces 2015, 7, 17765−17775

tissue resolution because of the similar electron density.[28] Whereas, noninvasive MRI exhibits high spatial resolution, unlimited penetration depth and provides excellent contrast for soft tissues;[29] however, it still suffers from somewhat low sensitivity.[30] Therefore, the combination of CT and MRI can deliver more accurate and comprehensive diagnostic information by combining the specific advantages of each technique. There are basically two approaches to achieve MRI/CT bimodal imaging. The first way is to design multimodal scanners, where a single device contains two different imaging modalities. However, developing this dedicated equipment and replacing the currently available individual MRI and CT facilities would become costly.[31] The alternative approach is the use of multimodal imaging contrast agents.[32] However, to achieve efficiently this goal, new synthetic methodologies must be developed in order to produce materials that provide efficient contrast, simultaneously, in both CT and MRI.

Gadolinium (Gd), possessing a large magnetic moment and unpaired electrons in the outer shell, performs as an excellent clinical positive contrast agent for MRI in the form of chelates.[33] Whereas, clinical contrast agents for CT are predominantly based on tri-iodobenzene, which can effectively absorb X-rays. Unfortunately, the short circulation time of the Gd chelates and iodinated compounds, owing to the nature of small molecules, can prevent the relative imaging technique from gathering the required information. Moreover, it is difficult to further functionalize the small molecules for targeting or other purposes (e.g., adding another imaging agent).[34,35] AuNPs have been demonstrated to be suitable as a contrast agent for CT imaging[34] due to their high atomic number, superior absorption coefficient, and tunable particle size and morphology. A number of studies[36−39] have reported the combination of Au nanospheres and Gd chelates for the preparation of multimodal MRI/CT contrast agents since the seminal work of Debouttière et al.[40] In addition, further studies, such as Gd-chelate-modified gold nanorods or nanospheres,[41−43] Gd-enriched DNA AuNPs conjugates,[44] and combining Gd chelates with gold nanostructures as multimodal MRI/CT contrast agents have been conducted. However, all of these reported Gd/Au-based multimodal contrast agents for MRI/CT imaging involve Gd chelate materials. Owing to the small sizes of Gd chelates and constant surface area of AuNPs (with given size and concentration), a low magnetic center (Gd^{3+}) payload per particle and limited further functionalization of AuNPs for the introduction of targeting or the improvement of biocompatibility impede their full potential in biomedical imaging application.[45] In contrast, Gd metal−organic framework (MOF) nanoparticles have a larger size and higher Gd^{3+} payload, thereby offering improved retention time and significantly higher relaxivities.[29] Also, GdMOF nanoparticles can be further functionalized with polymers to improve biocompatibility or with targeting ligands to make it possible for targeted diagnosis.[46]

In this study, on the basis of our previously developed technique for the modification of GdMOF nanoparticles with polymers prepared via reversible addition−fragmentation chain transfer (RAFT) polymerization,[46] we report for the first time the integration of GdMOF nanoparticles, rather than Gd chelates, with AuNPs through poly(acrylic acid) (PAA) chains that were attached to the GdMOF nanoparticles and acted as the active sites for interaction with Au ions. After the coordination of Au ions, a reducing agent was used to prepare AuNPs within the surface attached PAA. These hybrid GdMOF/Au nanocomposites, presenting both excellent MRI and CT responses, show potential application as a bimodal imaging contrast agent.

EXPERIMENTAL SECTION

Materials. Cetyltrimethylammonium bromide (CTAB) (99%), gadolinium(III) chloride hexahydrate ($GdCl_3·6H_2O$) (99.999%), terephthalic acid (98%), methylamine aqueous solution (40 wt %), sodium salicylate (NaSal) (99.5%), 2,2′-azobisisobutrylnitrile (AIBN) (98%), chloroauric acid ($HAuCl_4·3H_2O$), sodium borohydride ($NaBH_4$), and hexanol (98%) were purchased from Sigma-Aldrich. Heptane (HPLC grade) and *N*,*N*-dimethylformamide (DMF) (HPLC grade) were purchased from Mallinckrodt Chemicals. Deionized ultrafiltered (DIUF) water and ethanol were purchased from Fisher. Acrylic acid (AA) (stabilized with 200 ppm MEHQ, 99.5%) and hexylamine (99%) were purchased from Acros Chemicals. AA was distilled under vacuum and then stored in a freezer prior to use. AIBN was recrystallized twice from methanol prior to use. Unless otherwise noted, all other chemicals were used as received. ISOVUE Multipack-300 (30% organically bound iodine, lopamidol Injection 61%) was purchased from Bracco Diagnostics. Each mL of ISOVUE Multipack-300 provides 612 mg of iopamidol with 1 mg of tromethamine and 0.39 mg of edetate calcium disodium. Magnevist sterile solution (each mL contains 469.01 mg of gadopentetate dimeglumine, 0.99 mg of meglumine, and 0.40 mg of diethylenetriamine pentaacetic acid) was purchased from Berlex and used as received.

Characterization. Transmission electron microscopy (TEM) was performed on a Philips/FEICM200 with an accelerating voltage of 120 kV. UV−visible (UV−vis) spectroscopy was performed on a Thermo Electron Corp., Nicolet Evolution 300 BB spectrophotometer with a xenon light source and utilized standard 10 mm quartz cuvettes. Fourier transform infrared (FTIR) spectra were collected utilizing a Smart SAGA attachment coupled with a Thermo-Electron Nicolet 4700 spectrometer, collecting 16 background scans and 64 sample scans, and analyzed utilizing Nicolet's OMNIC software. ζ-Potential data for the nanoparticles dispersed in water was gathered from a NanoBrook ZetaPALS ζ-potential analyzer and Smoluchowski model (for aqueous solutions). Inductively coupled plasma atomic emission spectroscopy (ICP-AES) data was acquired on a PerkinElmer Optima 5300 ICP-AES instrument following the EPA 200.7 standardized method. The instrument was calibrated with an internal scandium standard and recalibrated if there was greater than 20% drift from the 50 ppm concentration. Samples were diluted in a 1% nitric acid solution to give a total volume of 10 mL and run against an internal quality control Gd standard (high purity standards) using a two point calibration. Matrix assisted laser desorption ionization time-of-flight mass spectrometry (MALDI-ToF MS) was employed to determine the molecular weight of the PAA. The PAA samples were prepared at 5 mg/mL in DIUF water in a sinapinic acid matrix at a mole ratio of 10 to 3. X-ray diffraction (XRD) on powder nanoparticle samples was performed on a Bruker D2 Phaser diffractometer using Cu Kα radiation. Thermogravimetric analysis (TGA) was performed using a TA Q500 equipped with a platinum pan and heated at a rate of 10 °C/min under air. MRI: Samples were placed into a 4.7 T Bruker Pharma Scan MRI with a 31 mm-diameter Bruker volume coil. RARE-VTR, to assess longitudinal relaxation time (T_1), scan parameters were as follows: field-of-view (FOV): 6 cm; slice thickness, 1.5 mm; repetition time (TR), 400, 500, 600, 700, 800, 900, 1000, 1500, 2000, 3000, 4000, 5000, 6500 ms; echo time (TE), 50 ms; number of slices, 2; number of averages, 2; matrix size, 128 × 128; flip angle, 180°; total acquisition time, 14.1 min. All images were analyzed with Bruker Paravision 3.0.2 software. For CT imaging, samples were placed into a Siemens Inveon positron emission tomography−computed tomography (PET/CT) scanner with low magnification. Scan parameters were as follows: tube voltage, 80 kVp; current, 500 uA; exposure time, 300 ms; magnification, Lo; binning, 4; total acquisition time, 5 min. Images were analyzed by AsiProVM to determine sample intensity.

Synthesis. *Preparation of Gadolinium Metal−Organic Framework (GdMOF) Nanoparticles.* The GdMOF nanoparticles were

DOI: 10.1021/acsami.5b03998
ACS Appl. Mater. Interfaces 2015, 7, 17765−17775

Scheme 1. Schematic of the Structures Produced[a]

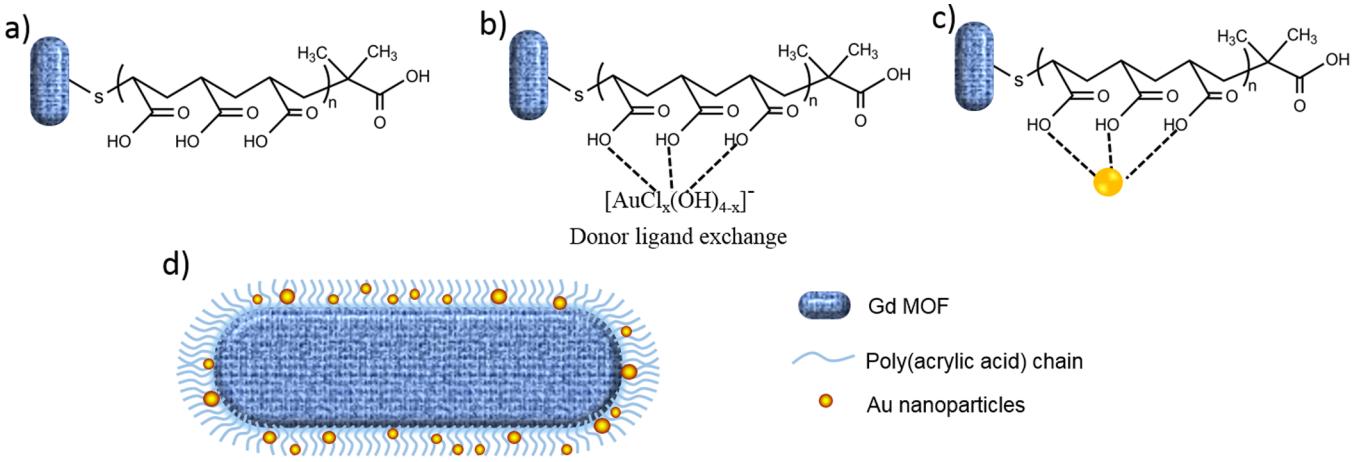

[a]After (a) deposition of PAA onto GdMOF nanostructures, (b) loading of Au ions onto PAA-modified GdMOF nanostructures, followed by (c) reduction of the Au ions to produce AuNPs entrapped in the surface immobilized PAA. (d) A schematic representation of the structure of hybrid GdMOF−PAA−Au nanostructures. The GdMOF core is shown in blue, the PAA chains as blue chains and the AuNPs in gold.

prepared using a variation of a method reported in the literature.[47] First, 10 g (0.06 mol) of terephthalic acid was dissolved in 8.34 mL of methylamine (40 wt % in water) solution and the resulting 1,4-benzenedicarboxylic acid (1,4-bdc) methylammonium salt was isolated via solvent removal under reduced pressure. Then 5 mL of 0.075 M (0.0856 g, 0.38 mmol) 1,4-bdc salt aqueous solution and 0.05 M (0.0929 g, 0.25 mmol) $GdCl_3$ aqueous solution were prepared separately. Next, 0.0352 g (0.22 mmol) of NaSal and 14.58 g (0.04 mol) of CTAB were mixed with 78.4 mL of 1-hexanol and 721.6 mL of heptane in a 1 L Pyrex bottle equipped with a stirring bar. After 10 min of vigorous stirring, 3.6 mL of 0.075 M 1,4-bdc salt solution was added into the system and the CTAB was allowed to dissolve. Finally, 3.6 mL of a 0.05 M $GdCl_3$ solution was added into the bottle. The solution was then stirred overnight followed by centrifugation at 5000 rpm for 20 min to remove surfactant and any unreacted reagents. After the supernatant was discarded, the nanoparticles were dispersed in 15 mL ethanol, sonicated, and then recentrifuged at 5000 rpm for 20 min. This was repeated two more times. The resulting particles were finally dispersed in 30 mL ethanol and used for further modification. This procedure produces one batch (0.05 g of nanoparticles dipersed in 30 mL of ethanol) of GdMOF nanoparticles.

Synthesis of Poly(acrylic acid) (PAA) via Reversible Addition−Fragmentation Chain Transfer (RAFT) Polymerization. It has been previously demonstrated that polymers prepared by RAFT polymerization yield a thiocarbonylthio end group functionality that can be reduced to a thiol and used for the deposition of the polymer onto GdMOF nanoparticles.[46,48] Therefore, the use of RAFT polymerization for preparation of the PAA was critical. The RAFT agent S-1-dodecyl S′-(α,α-dimethylacetic acid) trithiocarbonate (DATC) was synthesized and purified according to a literature procedure.[49] AA (40 mL, 0.583 mol) and DMF (90 mL) were added to a Schlenk flask and purged with high purity nitrogen in a dry ice bath for 30 min. The headspace of the flask was then purged with high purity nitrogen for 10 min. AIBN (0.0686 g, 0.418 mmol) and DATC (1.5239 g, 4.18 mmol) were weighed into a separate Schlenk flask and exposed to three vacuum and nitrogen purge cycles to remove air. The AA/DMF solution was then transferred to the AIBN/DATC flask via cannula and reacted for 9 h at 60 °C. The resulting polymer mixture was dried at room temperature overnight and then under vacuum at 100 °C to remove excess monomer and solvent. (conversion = 99.94%, $M_{n,theoretical}$ = 10 446 g/mol, $M_{n,experimental}$ = 9765 g/mol, and polydispersity index (PDI) = 1.1).

Modification of GdMOF Nanoparticles with PAA. Ethanol (20 mL) and 0.1 g of PAA were added to a 50 mL round-bottom flask, sealed, purged with high purity nitrogen for 30 min, and then left under nitrogen. 0.45 mL Hexylamine was added to the PAA solution via a syringe and allowed to stir for 1.5−2 h to facilitate reduction of the trithiocarbonate polymer end groups to thiol groups. 0.015 g GdMOF nanoparticles (9 mL out of a 30 mL batch) was mixed with 11 mL of ethanol and transferred into a 50 mL Schlenk flask equipped with a stir bar, sealed, purged with high purity nitrogen for 30 min and left under nitrogen. The reduced PAA solution was then transferred to the GdMOF nanoparticle solution via cannula and the reaction mixture stirred at room temperature under nitrogen for 24 h. After this time, the unattached polymer chains were removed via three centrifugations (5000 rpm, 20 min) with ethanol and once with water, to yield the PAA-modified GdMOF nanoparticles.

Synthesis of the Hybrid GdMOF−PAA−Au Nanocomposites. A 1/3 batch of the PAA deposited GdMOF nanoparticles (i.e., 0.005 g GdMOF nanoparticles) were dispersed in 10 mL of DIUF water in a 25 mL round-bottomed flask equipped with a stirring bar. Then, 0.44 mL of a 0.01 M gold precursor (0.0394 g, 0.1 mmol, $HAuCl_4{\cdot}3H_2O$ in 10 mL of DI water) aqueous solution was added into the flask with stirring. The mixture was then placed in a 60 °C oil bath and stirred for 24 h to facilitate the coordination between gold ions and PAA. After 24 h, the solution was taken out of the oil bath and cooled to room temparature. Next, 0.01 M sodium borohydride was prepared by dissolving 0.0019 g (0.0498 mmol) $NaBH_4$ in 10 mL of DIUF water in an ice bath. 10 mL of freshly prepared $NaBH_4$ solution was then added all at once into the flask. Stirring was continued for another 10 min. Centrifugation was then applied (5000 rpm, 20 min) one more time, washing with DIUF water.

Synthesize GdMOF Supported Au Nanocomposites. The procedure was the same as that used to synthesize the Gd−PAA−Au nanocomposites; however, the PAA-modified GdMOF nanoparticles were replaced with unmodified GdMOF nanoparticles. Briefly, 0.005 g (1/10 batch) of GdMOF nanoparticles was dispersed in 10 mL of DIUF water in a 25 mL round-bottomed flask, followed by the addition of 0.44 mL of a 0.01 M (0.0394 g, 0.1 mmol, $HAuCl_4{\cdot}3H_2O$ in 10 mL of DI water) gold precursor aqueous solution. The mixture was heated in a 60 °C oil bath for 24 h with stirring. Then, 10 mL of ice-cold freshly prepared 0.01 M (0.0019 g, 0.0498 mmol, in 10 mL of DIUF water) $NaBH_4$ solution was added to the solution. The reaction was stirred for another 10 min before cleaning. The resulting nanoparticles were cleaned by centrifugation (5000 rpm, 20 min), followed by one more wash with DIUF water.

RESULTS AND DISCUSSION

Although advances in biomedical imaging have been responsible for tremendous progress in clinical diagnosis, no single imaging technique includes all the required information for

DOI: 10.1021/acsami.5b03998
ACS Appl. Mater. Interfaces 2015, 7, 17765−17775

comprehensive biomedical diagnostics. In an effort to overcome these limitations, development of multimodal imaging contrast agents has become an emerging area of investigation. Among all the biomedical imaging modalities, CT is one of the most prevalent diagnostic tools in the clinic because of its cost effectiveness, wide availability, and anatomical imaging ability. However, it has limited soft tissue resolution. On the other hand, MRI offers superior contrast capability for soft tissues. To combine effectively MRI and CT together, new multimodal imaging agents need to be developed and, arguably, the best approach to produce these new materials is through nanoparticles. The vast majority of work previously conducted in the development of nanoparticle-based MRI/CT has focused on the use of AuNPs modified with Gd chelates. However, this approach typically leads to a low magnetic center (Gd^{3+}) payload per particle and limits further functionalization. To overcome these limitations, we describe a method to combine AuNPs and GdMOF nanoparticles via a polymer modification procedure. The development of these new nanocomposites not only offers excellent contrast in both CT and MRI, but also provides potentially longer circulation time in comparison with currently used small molecule contrast agents. To the best of our knowledge, this is the first report of using polymer-modified GdMOF nanoparticles for the preparation of multimodal imaging nanocomposites.

General Synthetic Route. A two-step protocol (Scheme 1), involving polymer modification of the surface of the GdMOF nanoparticles, was designed to increase the affinity between AuNPs and the GdMOF nanoparticles. In the first stage of this process, PAA is attached to the surface of the GdMOF nanoparticles via the modified end group of the polymer. The deposition of thiol-terminated polymer chains onto GdMOF nanoparticles was proposed and previously reported through the coordination of the thiolate end group with the vacant orbitals on the Gd^{3+} ions.[46] The second stage involves coordination of a Au salt to the carboxylate groups on the PAA and the subsequent reduction of the Au salt to Au nanoparticles. The Au nanoparticles are entrapped in the random coil structure of the surface immobilized PAA.[50] This forms what we will term a Gd−PAA−Au nanocomposite. The employment of PAA as a bridge will offer stronger interaction between GdMOF and AuNPs, which can resolve agglomeration issues experience by other systems, as discussed earlier.

Synthesis of GdMOF Nanoparticles. The GdMOF nanoparticles were synthesized using a variation of the reverse microemulsion process reported in the literature.[51] The magnetic center (Gd^{3+}) was provided via gadolinium chloride whereas the bridging ligand was 1,4-bdc. To obtain the desired morphology and prevent aggregation of the GdMOF nanoparticles, CTAB was introduced as the surfactant. A water to surfactant molar ratio of 10 was employed to yield nanoparticles that were 155 ± 30 nm in length and 30 ± 11 nm in width (Figures 1a,b). Powder XRD was utilized to determine the crystal structure of the GdMOF nanoparticles. The XRD pattern (Figure 3a black curve) showed that they were crystallized into a $Gd(1,4\text{-bdc})_{1.5}(H_2O)_2$ structure similar to the bulk phase of $Tb(1,4\text{-bdc})_{1.5}(H_2O)_2$ that has been previously reported.[52] Furthermore, the FTIR spectrum of the unmodified GdMOF nanoparticles (Figure 2a, black curve) showed the characteristic stretches of the carboxylate groups and aromatic ring of the 1,4-bdc bridging ligand at 1400, 1538, and 3065 cm^{-1} (black arrow in Figure 2b black curve). The coordinated water within the nanoparticle structure was also seen as a peak at 3460 cm^{-1}.

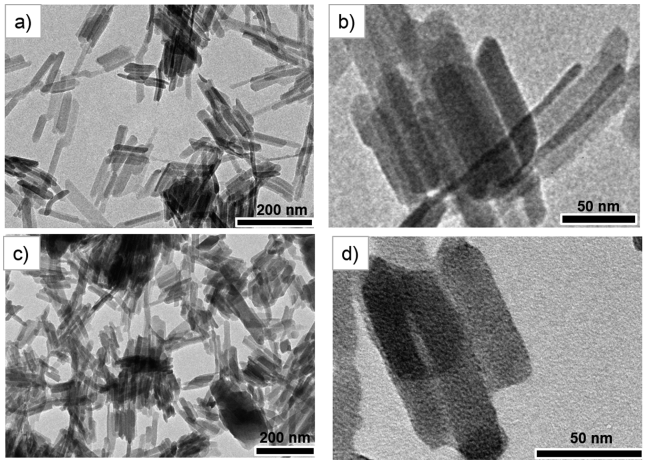

Figure 1. (a and b) TEM images of unmodified GdMOF nanoparticles, (c and d) TEM images of PAA-modified GdMOF nanoparticles.

Synthesis of PAA with RAFT Polymerization. PAA ($M_{n,theoretical}$ = 10 446 g/mol, $M_{n,experimental}$ = 9765 g/mol, and PDI = 1.1) with a trithiocarbonate end group was prepared via RAFT polymerization employing DATC as the RAFT agent. The FTIR spectrum of the homopolymer PAA is shown in Figure 2a (red curve). Interpretation of the spectrum shows two representative peaks at 1700 and 1635 cm^{-1}, which correspond to the carbonyl from the protonated and deprotonated form of the carboxylic acid group, respectively. In addition, the observed broad peak centered approximately at 3000 cm^{-1} (from 2500 to 3300 cm^{-1}) was attributed to the −OH stretch from the protonated form of the carboxylic acid group.

Surface Modification of GdMOF Nanoparticles with PAA. The trithiocarbonate end group of the RAFT prepared PAA was reduced to a thiol group using hexylamine,[53,54] creating an end group that can be used for deposition of the PAA chains onto the GdMOF nanoparticles (Scheme 1a). The prepared PAA-modified GdMOF nanoparticles were characterized using TEM, FTIR, TGA, and ζ-potential measurements. As can be seen in Figure 1c,d, the PAA coating on the nanoparticles is somewhat difficult to observe, as PAA and the GdMOF nanoparticles have a similar electron density and, hence, similar contrast in the TEM. However, comparing the FTIR spectra of the unmodified GdMOF, free PAA, and PAA-modified GdMOF nanoparticles (Figure 2a), it was demonstrated that PAA was successfully deposited to GdMOF surfaces. This is evidenced by the representative peak at 1700 cm^{-1} displayed in PAA-modified GdMOF (black arrows in Figure 2b for the blue curve), which comes from the carbonyl of the carboxylic acid groups of PAA. The fact that the intensity of this peak was much stronger than the unmodified GdMOF nanoparticles demonstrated the successful modification of GdMOF nanoparticles with PAA. In addition, the peaks around 2930 cm^{-1} for the C−H stretch of the polymer backbone were observed for the PAA-modified GdMOF sample. The broad OH stretch observed in the free PAA spectrum is not observed in the PAA-modified GdMOF spectrum due to the fact that the deposition process will result in deprotonation of the carboxylic acid group of the PAA. Finally, it should be mentioned that although the FTIR

DOI: 10.1021/acsami.5b03998
ACS Appl. Mater. Interfaces 2015, 7, 17765−17775

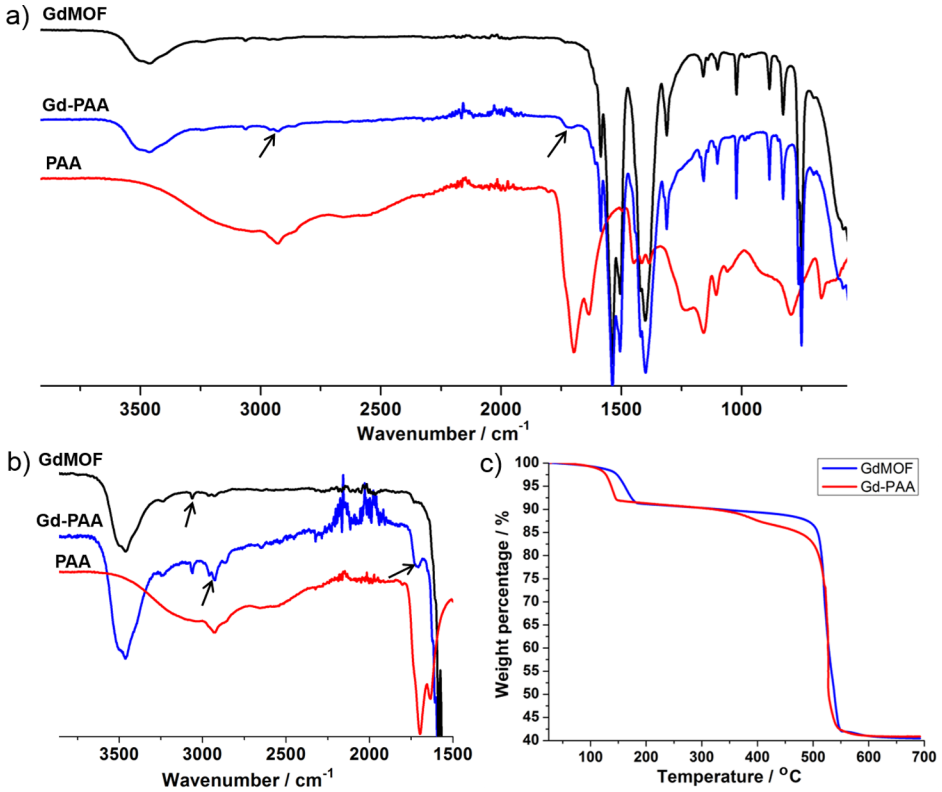

Figure 2. FTIR spectra of unmodified GdMOF nanoparticles (black), homopolymer PAA (red) and PAA-modified GdMOF nanoparticles (blue) from (a) 500−4000 cm^{-1} and (b) 1500−4000 cm^{-1}. (c) TGA of unmodified GdMOF nanoparticles (blue), and PAA-modified GdMOF nanoparticles (red).

spectrum clearly demonstrates the presence of the PAA on the surface of the GdMOF nanoparticles via the characteristic peaks discussed above, the thiolate end group of the PAA chains on the nanoparticles cannot be observed. This is due to several reasons: (1) the C−S bond is only present on one end of the PAA chains and is, therefore, difficult to detect in FTIR at such low concentrations; (2) the surface modification of the GdMOF nanoparticles with PAA is achieved via the "grafting to" technique, which has been reported to have lower grafting densities than the "grafting from" method,[55,56] and this will decrease the amount of polymer chains per nanoparticle, again, lowering the concentrations of the polymer end groups and making the C−S bond difficult to detect; and (3) the stretching vibration from the C−S bond is a weak absorption around 600−700 cm^{-1} and is thus typically hard to see, even in concentrated samples, and is not commonly used in structural determination. In addition, the FTIR spectra from previous literature involving the use of either the "grafting to" or "grafting from" technique for the modification of various nanoparticles using RAFT prepared polymers also does not observe the C−S bond.[57−60]

To demonstrate further the successful surface modification of the GdMOF nanoparticles with PAA, the ζ-potential of the particles, both unmodified and polymer-modified, in aqueous suspensions was determined. Before PAA modification, the surface charge for GdMOF nanoparticles was positive (13.0 ± 1.1 mV), which is mainly due to the Gd^{3+} at the surface of the nanoparticles. After the PAA was deposited on the GdMOF nanoparticles, the ζ-potential changed to negative (−9.1 ± 1.5 mV). The negative charge is a result of the carboxylate anions formed upon deprotonation of the carboxylic acid groups of the PAA (pK_a of approximately 4.5) in deionized water (pH = 6.57). It should be noted that we have previously demonstrated that the polymer-modified GdMOF nanoparticles have excellent stability, in terms of both nanoparticle structure and polymer film, in aqueous media and, indeed, the polymer coating on the GdMOF nanoparticles actually improves the stability in comparison to unmodified GdMOF nanoparticles.[48] Therefore, we would not expect any experiments or analysis performed in aqueous solution to adversely affect the nanoparticles.

To demonstrate further the attachment of the PAA to the GdMOF nanoparticles and also estimate the grafting density, TGA was performed. As shown in Figure 2c, both the unmodified GdMOF and PAA-modified GdMOF nanoparticles exhibited a weight loss around 130 to 200 °C, which was attributed to the coordinated water within the GdMOF nanoparticle structure. However, the PAA-modified GdMOF nanoparticles demonstrated a weight loss of approximately 7% between 350 and 500 °C that was not observed in the unmodified GdMOF nanoparticles. This weight loss difference was attributed to the PAA on the surface of the GdMOF nanoparticles, as it corresponds to the observed decomposition temperature of free PAA in TGA, and provides further evidence of successful polymer modification of the nanoparticles. The grafting density of PAA on the GdMOF nanoparticles was calculated by using the weight loss from TGA, the average size of the nanoparticles from TEM images (length = 155 nm and width = 33 nm) and the average molecular weight of PAA ($M_{n,experimental}$ = 9765 g/mol). The GdMOF nanoparticles were treated as cylindrical particles in the calculation and the bulk density of GdMOF nanoparticles was taken as 2.529 g/cm^{-3},

DOI: 10.1021/acsami.5b03998
ACS Appl. Mater. Interfaces 2015, 7, 17765−17775

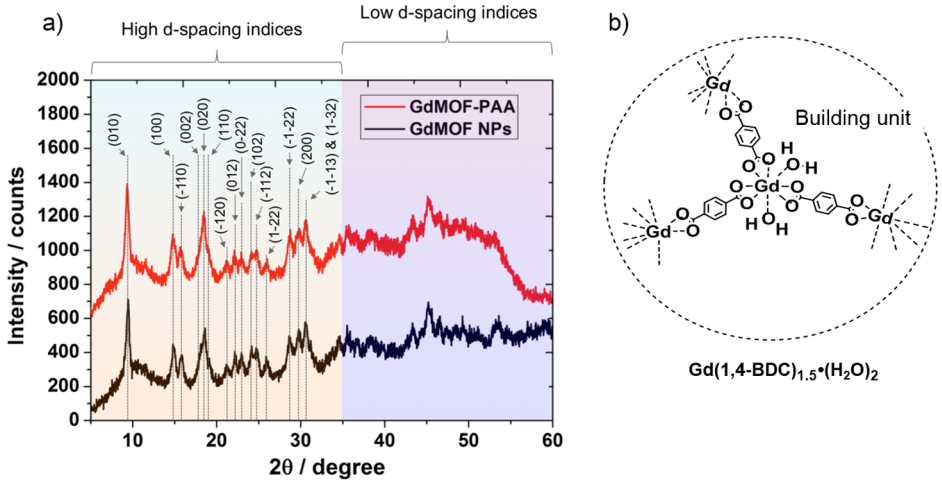

Figure 3. (a) XRD patterns for GdMOF nanoparticles before and after PAA modification. (b) Structure drawing illustrating the repeating unit for the GdMOF structure, $Gd(1,4\text{-}BDC)_{1.5}(H_2O)_2$.

based on a literature value.[46] From these calculations, the grafting density was determined to be 0.09 chains/nm^2. This value is slightly lower than polymer brush systems that are reported in the literature,[61] but it is reasonable when considering that the "grafting to" technique is used to modify the GdMOF nanoparticles and is comparable to values previously reported by our group using this method to surface modify GdMOF nanoparticles with RAFT prepared polymers.[46]

To demonstrate that the surface modification process does not change the morphology or structure of the GdMOF nanoparticles, different characterization techniques were carried out before and after the PAA modification. First of all, as shown in Figure 1c,d, the TEM images indicate that the GdMOF nanoparticles (compared to Figure 1a,b) have good morphological stability after going through the modification process. Moreover, XRD demonstrated that the peak positions and intensities were not significantly changed after PAA modification (Figure 3a, red curve). This was expected as the XRD peaks originate from the crystalline phase of the GdMOF nanoparticles, which does not change after surface modification, and the peak width is primarily determined by the size of the GdMOF nanoparticles, which also does not significantly change after surface modification due to the very thin layer of PAA present (approximately 3 nm). The combination of all of these results confirms that the PAA was successfully deposited on the surface of the GdMOF nanoparticles and that the structure and morphology of the GdMOF nanoparticles was well maintained.

Formation of AuNPs on PAA-Modified GdMOF Nanoparticles. The attachment of the PAA on the surface of the GdMOF nanoparticles allows for the binding of metal ions to the carboxylic acid functionality present on the PAA in aqueous solution. Subsequently, inorganic nanoparticles can be obtained and entrapped in the polymer chains by reduction of the metal-ion-modified PAA (Scheme 1).[50,62] Within this work, the goal is to produce a multimodal imaging agent that can be used for both MRI and CT imaging. As such, Au ions were used to modify the PAA on the surface of the GdMOF nanoparticles, so that Au nanoparticles could be formed after the reduction reaction. TEM images (Figure 4a) clearly show highly dispersed Au nanoparticles were formed on the PAA-modified GdMOF nanoparticles, with an average diameter of 4 ± 2 nm (Figure 4b), when $HAuCl_4$ precursor was used to load Au ions

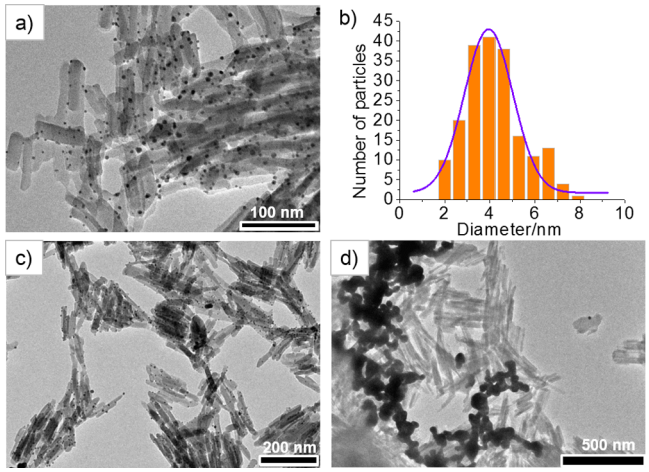

Figure 4. (a) TEM images of hybrid GdMOF−PAA−Au nanocomposite with $HAuCl_4$ as the gold precursor, where the darker (black) dots are the AuNPs. (b) Size distribution of AuNPs on PAA-modified GdMOF nanoparticles were analyzed by measuring the diameter of 200 AuNPs from TEM images. TEM images of (c) Gd−PAA−Au nanocomposites prepared with PAA modification at lower magnification and (d) unmodified GdMOF particles mixed directly with 0.44 mL of 0.01 M $HAuCl_4$ solution and followed by reduction.

onto the PAA. To show the importance of the PAA coating in producing the nanocomposite structure, coordination of Au ions to the unmodified GdMOF nanoparticles was attempted. These results show that when unmodified GdMOF nanoparticles are used in the same process, the majority of the GdMOF nanoparticles have no AuNPs attached and the presence of physically separated, large AuNPs was also observed (Figure 4d). Whereas, when the GdMOF nanoparticles are modified with PAA, small, uniform AuNPs are well dispersed on the surface of all of the nanoparticles (Figure 4c). Hence, it was concluded that the PAA deposition on GdMOF nanoparticles is a crucial step for both loading the Au ions and formation of the GdMOF−PAA−Au nanocomposite.

To characterize further this system, UV−vis spectra were collected for the unmodified GdMOF nanoparticles, the PAA-modified GdMOF nanoparticles, and the GdMOF−PAA−Au nanocomposite (Figure 5a). All three samples show a similar absorbance around 240 nm and a shoulder around 300 nm,

DOI: 10.1021/acsami.5b03998
ACS Appl. Mater. Interfaces 2015, 7, 17765−17775

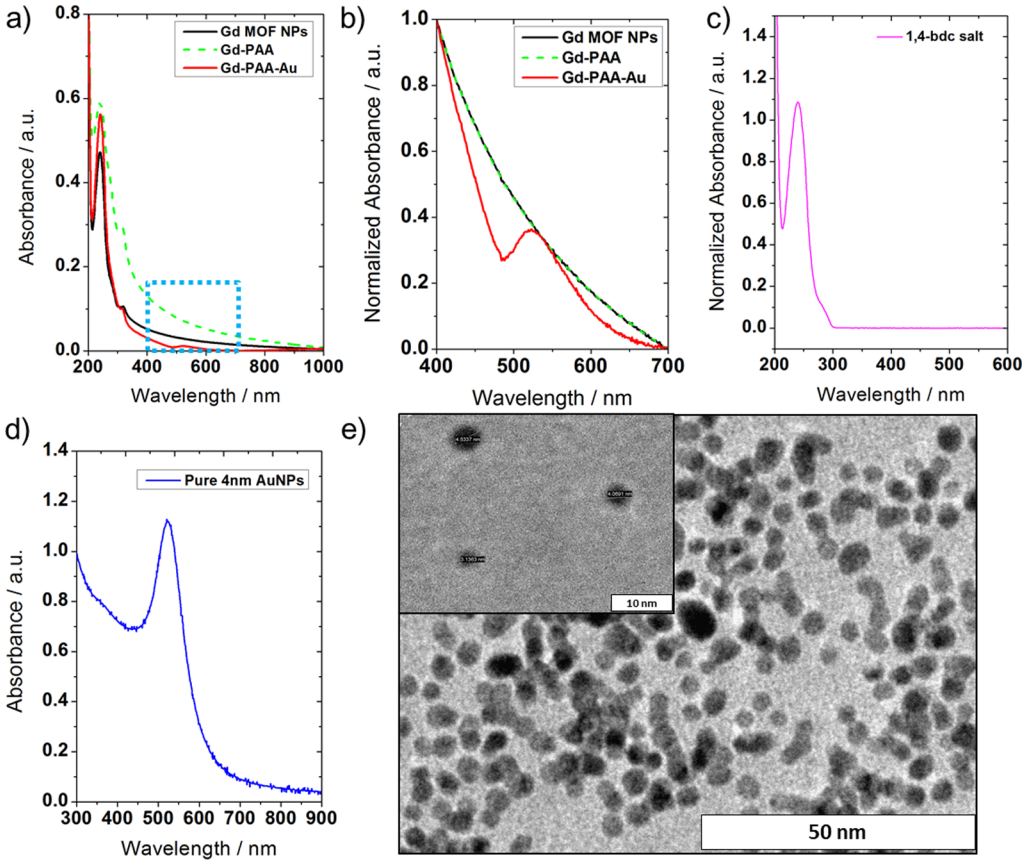

Figure 5. (a) UV−vis spectra of unmodified GdMOF (solid black curve), PAA-modified GdMOF (green dash curve), and hybrid GdMOF−PAA−Au nanocomposites (solid red curve). (b) Normalized and expanded UV−vis spectra of all three samples from the blue dashed rectangle in panel a. (c) UV−vis spectrum of 1,4-bdc methylammonium salt. (d) UV−vis spectrum of a solution of 4 nm AuNPs and (e) TEM images for the 4 nm AuNPs (inset is the TEM image with higher magnification).

which belong to the 1,4-bdc bridging ligand (the UV−vis spectrum of pure 1,4-bdc is shown in Figure 5c). However, while the UV−vis spectra of the unmodified and PAA-modified GdMOF nanoparticles then decline to baseline from 300 to 1000 nm, a small peak was observed around 520 nm for the GdMOF−PAA−Au nanocomposite. In order to clearly display this difference, the UV−vis spectra were normalized and expanded from 400 to 700 nm in Figure 5b. After normalization, the unmodified and the PAA-modified GdMOF nanoparticles show identical absorbance across this range, since the PAA has no absorbance at these wavelengths. However, the spectrum for the GdMOF−PAA−Au nanocomposite has a peak at 521 nm that was attributed to the presence of the AuNPs in the nanocomposite. To confirm this, 4 nm spherical AuNPs were synthesized independently (Figure 5e) and analyzed using UV−vis spectroscopy (Figure 5d). As can be seen, the spectra for the independent AuNPs matches the absorbance peak (approximately 520 nm) observed in the UV−vis spectrum of the GdMOF−PAA−Au nanocomposite (Figure 5b,d). As such, the size measured from the TEM images of the GdMOF−PAA−Au nanocomposite corresponds well with the UV−vis spectrum obtained for the nanocomposite.

MRI and CT Imaging Test. To evaluate the performance of the GdMOF−PAA−Au nanocomposites as a multimodal contrast agent for MRI and CT, a series of aqueous solutions at different dilutions were analyzed using a Bruker Pharma Scan MRI instrument at 4.7 T and a Siemens Inveon PET/CT scanner with low magnification at 80 kVp. The MRI results demonstrate qualitatively that with increasing Gd concentration (3.34, 15.75, and 33.4 ppm), the brightness of both the unmodified GdMOF nanoparticles and the GdMOF−PAA−Au nanocomposite increased (Figure 6a,b). These results also demonstrate that both the unmodified GdMOF nanoparticles and the GdMOF−PAA−Au nanocomposite offer brighter images than the clinically used chelate-based Gd contrast agent, Magnevist, even at lower Gd concentrations (Figure 6c). When comparing the modified and unmodified GdMOF nanoparticles, in each case, samples with a similar concentration of Gd demonstrated a similar contrast in MRI. To obtain quantitative comparison of the samples from the MRI studies, the longitudinal relaxation time (T_1) for each sample was determined and used to calculate the longitudinal relaxivity (r_1) for the different GdMOF nanoparticle systems (Figure 6d,e,f). The r_1 values for the unmodified GdMOF and the GdMOF−PAA−Au nanocomposite are 4.5 mM^{-1} s^{-1} and 4.9 mM^{-1} s^{-1}, respectively. The similar r_1 values indicate that the MRI contrast agent performance of the GdMOF−PAA−Au nanocomposite was not hindered by the surface modification procedure. Furthermore, the r_1 value of the clinically used Gd chelate Magnevist is 3.5 mM^{-1} s^{-1}, which is slightly lower than the nanocomposites. However, the r_1 values were much lower than the values reported in other work and our previous work,[46,47] which was mainly due to the differences in particle morphology and the magnetic field strength. The r_1 typically

DOI: 10.1021/acsami.5b03998
ACS Appl. Mater. Interfaces 2015, 7, 17765−17775

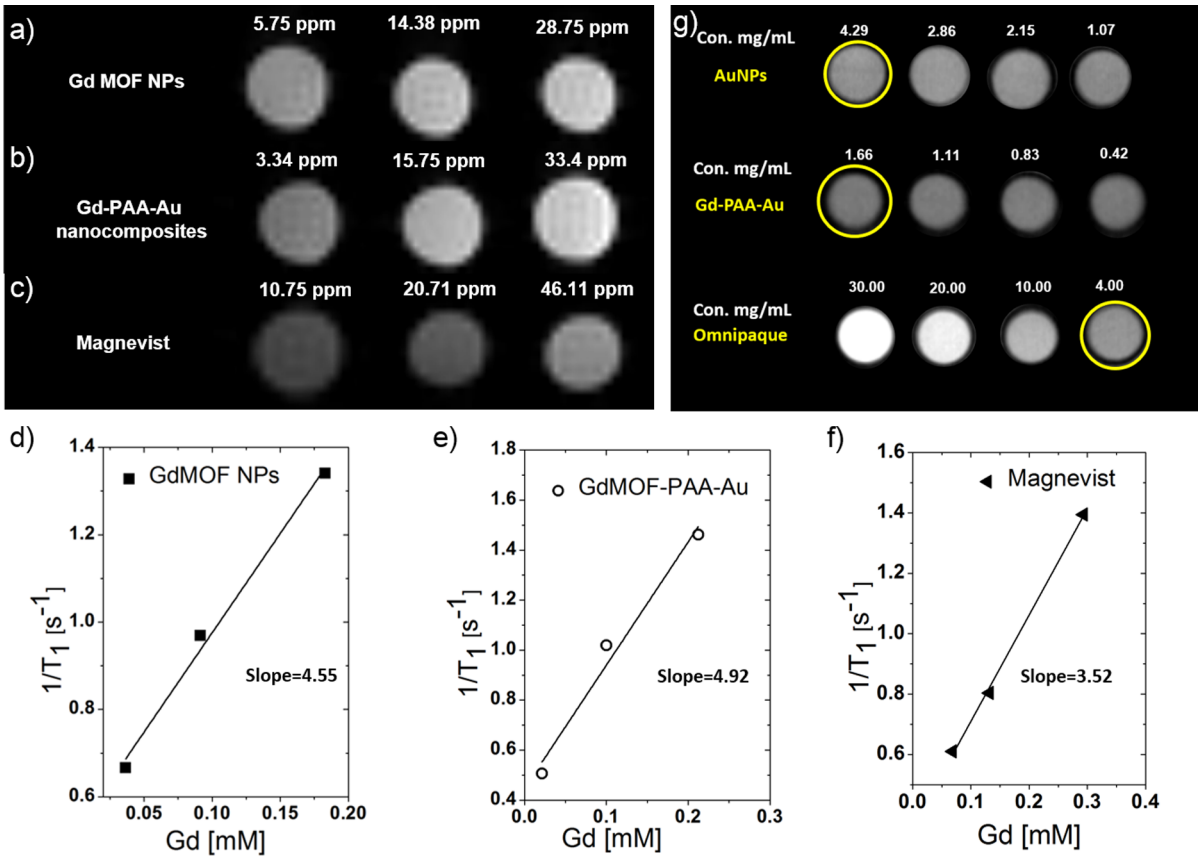

Figure 6. T_1-weighted MRI images of (a) unmodified GdMOF nanoparticles, (b) GdMOF−PAA−Au nanocomposite, and (c) chelate-based Gd contrast agent (Magnevist) at various Gd concentrations in DIUF water. Relaxation rate ($1/T_1$) of (d) unmodified GdMOF nanoparticles and (e) GdMOF−PAA−Au nanocomposite, and (f) chelate-based Gd contrast agent (Magnevist) as a function of the Gd concentration. (g) CT images of plain AuNPs, GdMOF−PAA−Au nanocomposite, and the iodine-based contrast agent Omnipaque with different Au or iodine concentrations. All concentrations are listed on top of each sample's CT image.

decreases with increasing magnetic field[63] and changes with various particles sizes.[45]

To determine the effectiveness of the GdMOF−PAA−Au nanocomposite as an imaging agent for CT, images were gathered by dispersion of the Gd−PAA−Au nanocomposites in water with different overall concentrations of Au. The results were also compared with the clinically used iodine-based CT contrast agent Omnipaque and with plain 12 nm AuNPs. The 12 nm AuNPs were used rather than 4 nm AuNPs, which have similar size as the AuNPs in the nanocomposites, because the need for ultrahigh centrifuge speed to separate and purify the 4 nm AuNPs prevented obtaining a high enough concentration (approximately 2 mg/mL or above) for CT analysis. In addition, use of 12 nm AuNPs should provide a reasonable comparison because CT contrast is primarily influenced by the concentration of AuNPs used and not their size or shape.[64] The unmodified GdMOF nanoparticles were not used as a comparison as preliminary testing demonstrated that they gave no significant signal in the CT instrument. This was expected as Au has a significantly higher X-ray attenuation than Gd and even though the Gd has a maximum X-ray mass attenuation coefficient of 3.11 $cm^2\ g^{-1}$ at its K-edge of 50.2 keV, the X-ray mass attenuation coefficient decays as you move away from the K-edge. As such, the X-ray mass attenuation coefficient is expected to be low at the 80 keV used in these studies.

As shown in Figure 6g, the GdMOF−PAA−Au nanocomposite show promising CT contrast capability, even at low Au concentration (1.66 mg/mL). Also observed in Figure 6g, the plain AuNPs (4.29 mg/mL Au concentration) and the clinically used iodine contrast agent Omnipaque (4.00 mg/mL I concentration) provide a similar contrast at similar concentrations. Given the similar brightness in the images, the attenuation values observed for Gd−PAA−Au nanocomposites and bare AuNPs are higher than omnipaue with similar concentrations. The CT attenuation numbers (Hounsfield unit, HU) for AuNPs (2.86 mg/mL Au) and Gd−PAA−Au nanocomposites (1.66 mg/mL Au) were 220.3 HU and 112.5 HU respectively. The number for Omnipaue at 4 mg/mL only reaches 208.3 HU. Although it appears that the GdMOF−PAA−Au nanocomposite provides lower contrast in the CT imaging, it is difficult to prepare samples of higher Au concentration due to the structure of the nanocomposite and the test environment for the CT imaging. However, the results for the GdMOF−PAA−Au nanocomposite at a Au concentration of 1.66 mg/mL were comparable to the plain AuNPs at similar concentrations and we also envision that the contrast could be further improved by increasing the Au concentration by using larger analysis tubes for the CT imaging.

CONCLUSIONS

We have reported the preparation of a dual-modal imaging contrast agent, Gd−PAA−Au nanocomposite, which can be

DOI: 10.1021/acsami.5b03998
ACS Appl. Mater. Interfaces 2015, 7, 17765−17775

used in both MRI and CT. The Gd−PAA−Au nanocomposites were successfully synthesized through deposition of PAA onto the surface of GdMOF nanoparticles followed by coordination and reduction of Au ions. Results demonstrated that the PAA was critical to the formation of the AuNPs on the GdMOF nanoparticles. The formed AuNPs were highly dispersed on surface of the GdMOF nanoparticles, with an average diameter of 4 nm. The hydrophilic PAA not only serves as the template of AuNPs, but also allows for access of water molecules to the surface of the GdMOF nanoparticles to promote interaction with Gd^{3+} ions. To demonstrate the effectiveness of the Gd−PAA−Au nanocomposites, MRI results show that the r_1 was 4.9 mM^{-1} s^{-1}, which is close to that of the unmodified GdMOF nanoparticles (r_1 = 4.5 mM^{-1} s^{-1}) and better that the clinically used MRI contrast agent Magnevist. Meanwhile, the Gd−PAA−Au nanocomposites also enhance the contrast of CT imaging, even when the Au concentration is as low as 1.66 mg/mL.

AUTHOR INFORMATION

Corresponding Author

*S. G. Boyes. E-mail: sboyes@mines.edu.

Funding

The authors thank the State of Colorado for providing a Bioscience Discovery Evaluation Proof of Concept Grant and the Colorado School of Mines for providing a Proof of Concept grant to support this work.

Notes

The authors declare no competing financial interest.

ACKNOWLEDGMENTS

We thank Dr. Natalie Serkova and Kendra Huber from University of Colorado Denver for their help with MRI and CT imaging test.

ABBREVIATIONS

AuNPs, gold nanoparticles
DATC, S-1-dodecyl S′-(α,α′-dimethylacetic acid) trithiocarbonate
MRI, magnetic resonance imaging
CT, computed tomography
SPECT, single photon emission computed tomography
PET, positron emission tomography
GdMOF, gadolinium metal−organic framework
PAA, poly(acrylic acid)
RAFT, reversible addition−fragmentation chain transfer
TEM, transmission electron microscopy
FTIR, Fourier transform infrared
ICP-AES inductively coupled plasma atomic emission spectroscopy
MALDI-ToF MS, matrix assisted laser desorption ionization time-of-flight mass spectrometry
XRD, X-ray diffraction
TGA, thermogravimetric analysis
T_1, longitudinal relaxation time
FOV, field-of-view
TR, repetition time
TE, echo time
CTAB, cetyltrimethylammonium bromide
AIBN, 2,2′-azobisisobutrylnitrile
DMF, *N*,*N*-dimethylformamide

REFERENCES

(1) Jeon, K.-J.; Moon, H. R.; Ruminski, A. M.; Jiang, B.; Kisielowski, C.; Bardhan, R.; Urban, J. J. Air-Stable Magnesium Nanocomposites Provide Rapid and High-Capacity Hydrogen Storage without Using Heavy-Metal Catalysts. *Nat. Mater.* **2011**, *10*, 286−290.

(2) Xuan, S.; Wang, Y.-X. J.; Yu, J. C.; Leung, K. C.-F. Preparation, Characterization, and Catalytic Activity of Core/shell Fe3O4@polyaniline@au Nanocomposites. *Langmuir* **2009**, *25*, 11835−11843.

(3) Subramanian, V.; Wolf, E. E.; Kamat, P. V. Catalysis with TiO2/gold Nanocomposites. Effect of Metal Particle Size on the Fermi Level Equilibration. *J. Am. Chem. Soc.* **2004**, *126*, 4943−4950.

(4) Lin, F.; Yang, J.; Lu, S.-H.; Niu, K.-Y.; Liu, Y.; Sun, J.; Du, X.-W. Laser Synthesis of Gold/oxide Nanocomposites. *J. Mater. Chem.* **2010**, *20*, 1103−1106.

(5) Zhou, T.; Lu, M.; Zhang, Z.; Gong, H.; Chin, W. S.; Liu, B. Synthesis and Characterization of Multifunctional FePt/ZnO Core/shell Nanoparticles. *Adv. Mater.* **2010**, *22*, 403−406.

(6) Wu, H.; Zheng, G.; Liu, N.; Carney, T. J.; Yang, Y.; Cui, Y. Engineering Empty Space between Si Nanoparticles for Lithium-Ion Battery Anodes. *Nano Lett.* **2012**, *12*, 904−909.

(7) Choi, H. S.; Liu, W.; Liu, F.; Nasr, K.; Misra, P.; Bawendi, M. G.; Frangioni, J. V. Design Considerations for Tumour-Targeted Nanoparticles. *Nat. Nanotechnol.* **2010**, *5*, 42−47.

(8) Hao, R.; Xing, R.; Xu, Z.; Hou, Y.; Gao, S.; Sun, S. Synthesis, Functionalization, and Biomedical Applications of Multifunctional Magnetic Nanoparticles. *Adv. Mater.* **2010**, *22*, 2729−2742.

(9) Gao, J.; Gu, H.; Xu, B. Multifunctional Magnetic Nanoparticles: Design, Synthesis, and Biomedical Applications. *Acc. Chem. Res.* **2009**, *42*, 1097−1107.

(10) Yoon, T.-J.; Kim, J. S.; Kim, B. G.; Yu, K. N.; Cho, M.-H.; Lee, J.-K. Multifunctional Nanoparticles Possessing A Magnetic Motor Effect for Drug or Gene Delivery. *Angew. Chem.* **2005**, *117*, 1092−1095.

(11) Liong, M.; Lu, J.; Kovochich, M.; Xia, T.; Ruehm, S. G.; Nel, A. E.; Tamanoi, F.; Zink, J. I. Multifunctional Inorganic Nanoparticles for Imaging, Targeting, and Drug Delivery. *ACS Nano* **2008**, *2*, 889−896.

(12) Jin, Y.; Jia, C.; Huang, S.-W.; O'Donnell, M.; Gao, X. Multifunctional Nanoparticles as Coupled Contrast Agents. *Nat. Commun.* **2010**, *1*, 41.

(13) Gao, X.; Cui, Y.; Levenson, R. M.; Chung, L. W. K.; Nie, S. In Vivo Cancer Targeting and Imaging with Semiconductor Quantum Dots. *Nat. Biotechnol.* **2004**, *22*, 969−976.

(14) Park, K.; Lee, S.; Kang, E.; Kim, K.; Choi, K.; Kwon, I. C. New Generation of Multifunctional Nanoparticles for Cancer Imaging and Therapy. *Adv. Funct. Mater.* **2009**, *19*, 1553−1566.

(15) Cheng, L.; Yang, K.; Li, Y.; Zeng, X.; Shao, M.; Lee, S.-T.; Liu, Z. Multifunctional Nanoparticles for Upconversion luminescence/MR Multimodal Imaging and Magnetically Targeted Photothermal Therapy. *Biomaterials* **2012**, *33*, 2215−2222.

(16) Melancon, M. P.; Zhou, M.; Li, C. Cancer Theranostics with near-Infrared Light-Activatable Multimodal Nanoparticles. *Acc. Chem. Res.* **2011**, *44*, 947−956.

(17) Liao, H.; Nehl, C. L.; Hafner, J. H. Biomedical Applications of Plasmon Resonant Metal Nanoparticles. *Nanomedicine (London, U. K.)* **2006**, *1*, 201−208.

(18) Cormode, D. P.; Jarzyna, P. A.; Mulder, W. J. M.; Fayad, Z. A. Modified Natural Nanoparticles as Contrast Agents for Medical Imaging. *Adv. Drug Delivery Rev.* **2010**, *62*, 329−338.

(19) Lok, C.-N.; Zou, T.; Zhang, J.-J.; Lin, I. W.-S.; Che, C.-M. Controlled-Release Systems for Metal-Based Nanomedicine: Encapsulated/self-Assembled Nanoparticles of Anticancer gold(III)/platinum-(II) Complexes and Antimicrobial Silver Nanoparticles. *Adv. Mater.* **2014**, *26*, 5550−5557.

(20) Mahmoud, W. E.; Bronstein, L. M.; Al-Hazmi, F.; Al-Noaiser, F.; Al-Ghamdi, A. A. Development of Fe/Fe3O4 Core-Shell Nanocubes as a Promising Magnetic Resonance Imaging Contrast Agent. *Langmuir* **2013**, *29*, 13095−13101.

(21) Bridot, J.-L.; Faure, A.-C.; Laurent, S.; Rivière, C.; Billotey, C.; Hiba, B.; Janier, M.; Josserand, V.; Coll, J.-L.; Elst, L. Vander; *et al.*

DOI: 10.1021/acsami.5b03998
ACS Appl. Mater. Interfaces 2015, 7, 17765−17775

Hybrid Gadolinium Oxide Nanoparticles: Multimodal Contrast Agents for in Vivo Imaging. *J. Am. Chem. Soc.* **2007**, *129*, 5076−5084.
(22) Kairdolf, B. A.; Smith, A. M.; Stokes, T. H.; Wang, M. D.; Young, A. N.; Nie, S. Semiconductor Quantum Dots for Bioimaging and Biodiagnostic Applications. *Annu. Rev. Anal. Chem.* **2013**, *6*, 143−162.
(23) Kim, J.; Piao, Y.; Hyeon, T. Multifunctional Nanostructured Materials for Multimodal Imaging, and Simultaneous Imaging and Therapy. *Chem. Soc. Rev.* **2009**, *38*, 372−390.
(24) Englmeier, K.-H.; Seemann, M. D. Multimodal Virtual Bronchoscopy Using PET/CT Images. *Comput. Aided Surg.* **2008**, *13*, 106−113.
(25) Raylman, R. R.; Majewski, S.; Lemieux, S. K.; Velan, S. S.; Kross, B.; Popov, V.; Smith, M. F.; Weisenberger, A. G.; Zorn, C.; Marano, G. D. Simultaneous MRI and PET Imaging of a Rat Brain. *Phys. Med. Biol.* **2006**, *51*, 6371−6379.
(26) Koral, K. F.; Zasadny, K. R.; Kessler, M. L.; Luo, J. Q.; Buchbinder, S. F.; Kaminski, M. S.; Francis, I.; Wahl, R. L. CT-SPECT Fusion plus Conjugate Views for Determining Dosimetry in Iodine-131-Monoclonal Antibody Therapy of Lymphoma Patients. *J. Nucl. Med.* **1994**, *35*, 1714−1720.
(27) Larson, T. A.; Bankson, J.; Aaron, J.; Sokolov, K. Hybrid Plasmonic Magnetic Nanoparticles as Molecular Specific Agents for MRI/optical Imaging and Photothermal Therapy of Cancer Cells. *Nanotechnology* **2007**, *18*, 325101.
(28) Mahmoudi, M.; Serpooshan, V.; Laurent, S. Engineered Nanoparticles for Biomolecular Imaging. *Nanoscale* **2011**, *3*, 3007−3026.
(29) Lin, W.; Hyeon, T.; Lanza, G. M.; Zhang, M.; Meade, T. J. Magnetic Nanoparticles for Early Detection of Cancer by Magnetic Resonance Imaging. *MRS Bull.* **2009**, *34*, 441−448.
(30) Mahmoudi, M.; Serpooshan, V.; Laurent, S. Engineered Nanoparticles for Biomolecular Imaging. *Nanoscale* **2011**, *3*, 3007−3026.
(31) Azhari, H.; Edelman, R. R.; Townsend, D. Multimodal Imaging and Hybrid Scanners. *Int. J. Biomed. Imaging* **2007**, *2007*, 45353.
(32) De Rosales, R. T. M. Potential Clinical Applications of Bimodal PET-MRI or SPECT-MRI Agents. *J. Labelled Compd. Radiopharm.* **2014**, *57*, 298−303.
(33) Liu, L.; Ding, H.; Yong, K.-T.; Roy, I.; Law, W.-C.; Kopwitthaya, A.; Kumar, R.; Erogbogbo, F.; Zhang, X.; Prasad, P. N. Application of Gold Nanorods for Plasmonic and Magnetic Imaging of Cancer Cells. *Plasmonics* **2011**, *6*, 105−112.
(34) Hainfeld, J. F.; Slatkin, D. N.; Focella, T. M.; Smilowitz, H. M. Gold Nanoparticles: A New X-Ray Contrast Agent. *Br. J. Radiol.* **2006**, *79*, 248−253.
(35) Popovtzer, R.; Agrawal, A.; Kotov, N. A.; Popovtzer, A.; Balter, J.; Carey, T. E.; Kopelman, R. Targeted Gold Nanoparticles Enable Molecular CT Imaging of Cancer. *Nano Lett.* **2008**, *8*, 4593−4596.
(36) Park, J.-A.; Reddy, P. a N.; Kim, H.-K.; Kim, I.-S.; Kim, G.-C.; Chang, Y.; Kim, T.-J. Gold Nanoparticles Functionalised by Gd-Complex of DTPA-Bis(amide) Conjugate of Glutathione as an MRI Contrast Agent. *Bioorg. Med. Chem. Lett.* **2008**, *18*, 6135−6137.
(37) Sk Md, N.; Kim, H.-K.; Park, J.-A.; Chang, Y.-M.; Kim, T.-J. Gold Nanoparticles Coated with Gd-Chelate as a Potential CT/MRI Bimodal Contrast Agent. *Bull. Korean Chem. Soc.* **2010**, *31*, 1177−1181.
(38) Kim, H.-K.; Jung, H.-Y.; Park, J.-A.; Huh, M.-I.; Jung, J.-C.; Chang, Y.; Kim, T.-J. Gold Nanoparticles Coated with Gadolinium-DTPA-Bisamide Conjugate of Penicillamine (Au@GdL) as a T1-Weighted Blood Pool Contrast Agent. *J. Mater. Chem.* **2010**, *20*, 5411−5417.
(39) Alric, C.; Taleb, J.; Le Duc, G.; Mandon, C.; Billotey, C.; Le Meur-Herland, A.; Brochard, T.; Vocanson, F.; Janier, M.; Perriat, P.; et al. Gadolinium Chelate Coated Gold Nanoparticles as Contrast Agents for Both X-Ray Computed Tomography and Magnetic Resonance Imaging. *J. Am. Chem. Soc.* **2008**, *130*, 5908−5915.
(40) Debouttière, P.-J.; Roux, S.; Vocanson, F.; Billotey, C.; Beuf, O.; Favre-Réguillon, A.; Lin, Y.; Pellet-Rostaing, S.; Lamartine, R.; Perriat, P.; et al. Design of Gold Nanoparticles for Magnetic Resonance Imaging. *Adv. Funct. Mater.* **2006**, *16*, 2330−2339.
(41) Sun, H.; Yuan, Q.; Zhang, B.; Ai, K.; Zhang, P.; Lu, L. Gd(III) Functionalized Gold Nanorods for Multimodal Imaging Applications. *Nanoscale* **2011**, *3*, 1990−1996.
(42) Luo, T.; Huang, P.; Gao, G.; Shen, G.; Fu, S.; Cui, D.; Zhou, C.; Ren, Q. Mesoporous Silica-Coated Gold Nanorods with Embedded Indocyanine Green for Dual Mode X-Ray CT and NIR Fluorescence Imaging. *Opt. Express* **2011**, *19*, 17030−17039.
(43) Lim, Y. T.; Cho, M. Y.; Choi, B. S.; Lee, J. M.; Chung, B. H. Paramagnetic Gold Nanostructures for Dual Modal Bioimaging and Phototherapy of Cancer Cells. *Chem. Commun. (Cambridge, U. K.)* **2008**, 4930−4932.
(44) Song, Y.; Xu, X.; MacRenaris, K. W.; Zhang, X.-Q.; Mirkin, C. A.; Meade, T. J. Multimodal Gadolinium-Enriched DNA-Gold Nanoparticle Conjugates for Cellular Imaging. *Angew. Chem., Int. Ed.* **2009**, *48*, 9143−9147.
(45) Hatakeyama, W.; Sanchez, T. J.; Rowe, M. D.; Serkova, N. J.; Liberatore, M. W.; Boyes, S. G. Synthesis of Gadolinium Nanoscale Metal-Organic Framework with Hydrotropes: Manipulation of Particle Size and Magnetic Resonance Imaging Capability. *ACS Appl. Mater. Interfaces* **2011**, *3*, 1502−1510.
(46) Rowe, M. D.; Chang, C.-C.; Thamm, D. H.; Kraft, S. L.; Harmon, J. F.; Vogt, A. P.; Sumerlin, B. S.; Boyes, S. G. Tuning the Magnetic Resonance Imaging Properties of Positive Contrast Agent Nanoparticles by Surface Modification with RAFT Polymers. *Langmuir* **2009**, *25*, 9487−9499.
(47) Rieter, W. J.; Taylor, K. M. L.; An, H.; Lin, W.; Lin, W. Nanoscale Metal-Organic Frameworks as Potential Multimodal Contrast Enhancing Agents. *J. Am. Chem. Soc.* **2006**, *128*, 9024−9025.
(48) Rowe, M. D.; Thamm, D. H.; Kraft, S. L.; Boyes, S. G. Polymer-Modified Gadolinium Metal-Organic Framework Nanoparticles Used as Multifunctional Nanomedicines for the Targeted Imaging and Treatment of Cancer. *Biomacromolecules* **2009**, *10*, 983−993.
(49) Lai, J. T.; Filla, D.; Shea, R. Functional Polymers from Novel Carboxyl-Terminated Trithiocarbonates as Highly Efficient RAFT Agents. *Macromolecules* **2002**, *35*, 6754−6756.
(50) Boyes, S. G.; Akgun, B.; Brittain, W. J.; Foster, M. D. Synthesis, Characterization, and Properties of Polyelectrolyte Block Copolymer Brushes Prepared by Atom Transfer Radical Polymerization and Their Use in the Synthesis of Metal Nanoparticles. *Macromolecules* **2003**, *36*, 9539−9548.
(51) Taylor, K. M. L.; Jin, A.; Lin, W. Surfactant-Assisted Synthesis of Nanoscale Gadolinium Metal-Organic Frameworks for Potential Multimodal Imaging. *Angew. Chem., Int. Ed.* **2008**, *47*, 7722−7725.
(52) Reineke, T. M.; Eddaoudi, M.; Fehr, M.; Kelley, D.; Yaghi, O. M. From Condensed Lanthanide Coordination Solids to Microporous Frameworks Having Accessible Metal Sites. *J. Am. Chem. Soc.* **1999**, *121*, 1651−1657.
(53) Sumerlin, B. S.; Lowe, A. B.; Stroud, P. A.; Zhang, P.; Urban, M. W.; McCormick, C. L. Modification of Gold Surfaces with Water-Soluble (Co)polymers Prepared via Aqueous Reversible Addition−Fragmentation Chain Transfer (RAFT) Polymerization †. *Langmuir* **2003**, *19*, 5559−5562.
(54) Hotchkiss, J. W.; Lowe, A. B.; Boyes, S. G. Surface Modification of Gold Nanorods with Polymers Synthesized by Reversible Addition−Fragmentation Chain Transfer Polymerization. *Chem. Mater.* **2007**, *19*, 6−13.
(55) Advincula, R. C.; Brittain, W. J.; Caster, K. C.; Ruhe, J. *Polymer Brushes: Synthesis, Characterization, Applications*; Wiley-VCH Verlag GmbH & Co.: Weinheim, 2005.
(56) Boyes, S. G.; Granville, A. M.; Baum, M.; Akgun, B.; Mirous, B. K.; Brittain, W. J. Polymer Brushes−−surface Immobilized Polymers. *Surf. Sci.* **2004**, *570*, 1−12.
(57) Chen, F.; Jiang, X.; Kuang, T.; Chang, L.; Fu, D.; Yang, J.; Fan, P.; Zhong, M. Polyelectrolyte/mesoporous Silica Hybrid Materials for the High Performance Multiple-Detection of pH Value and Temperature. *Polym. Chem.* **2015**, *6*, 3529−3536.

DOI: 10.1021/acsami.5b03998
ACS Appl. Mater. Interfaces 2015, 7, 17765−17775

(58) Kiani, K.; Hill, D. J. T.; Rasoul, F.; Whittaker, M.; Rintoul, L. Raft Mediated Surface Grafting Oft-Butyl Acrylate onto an Ethylene–propylene Copolymer Initiated by Gamma Radiation. *J. Polym. Sci., Part A: Polym. Chem.* **2007**, *45*, 1074–1083.
(59) Maleki, H.; Durães, L.; Portugal, A. Synthesis of Mechanically Reinforced Silica Aerogels via Surface-Initiated Reversible Addition-Fragmentation Chain Transfer (RAFT) Polymerization. *J. Mater. Chem. A* **2015**, *3*, 1594–1600.
(60) Li, Q.; Zhang, L.; Bai, L.; Zhang, Z.; Zhu, J.; Zhou, N.; Cheng, Z.; Zhu, X. Multistimuli-Responsive Hybrid Nanoparticles with Magnetic Core and Thermoresponsive Fluorescence-Labeled Shell via Surface-Initiated RAFT Polymerization. *Soft Matter* **2011**, *7*, 6958.
(61) Zhang, J. *Switchable and Responsive Surfaces and Materials for Biomedical Applications*; Elsevier Science: Amsterdam, 2014; p 324.
(62) Hotchkiss, J. W.; Mohr, B. G. R.; Boyes, S. G. Gold Nanorods Surface Modified with Poly(acrylic Acid) as a Template for the Synthesis of Metallic Nanoparticles. *J. Nanopart. Res.* **2010**, *12*, 915–930.
(63) Caravan, P.; Farrar, C. T.; Frullano, L.; Uppal, R. Influence of Molecular Parameters and Increasing Magnetic Field Strength on Relaxivity of Gadolinium- and Manganese-Based T1 Contrast Agents. *Contrast Media Mol. Imaging* **2009**, *4*, 89–100.
(64) Lee, N.; Choi, S. H.; Hyeon, T. Nano-Sized CT Contrast Agents. *Adv. Mater.* **2013**, *25*, 2641–2660.

DOI: 10.1021/acsami.5b03998
ACS Appl. Mater. Interfaces 2015, 7, 17765–17775